electronics

MDPI

Article

Multiport Isolated link with Current-Fed Z-Source Converters to Manage Power Imbalance in PV Applications

Jose M. Sandoval [1], Victor Cardenas [1,*], Manuel A. Barrios [1], Mario Gonzalez Garcia [2] and Janeth Alcala [3]

[1] Engineering Department, Autonomous University of San Luis Potosi, Dr. Manuel Nava No. 8, Col. Zona Universitaria Poniente, San Luis Potosí 78290, Mexico
[2] Engineering Department, Conacyt-Autonomous University of San Luis Potosi, San Luis Potosí 78290, Mexico
[3] Faculty of Electromechanical Engineering, University of Colima, Manzanillo, Colima 28864, Mexico
* Correspondence: vcardena@uaslp.mx

Received: 29 December 2019; Accepted: 30 January 2020; Published: 6 February 2020

check for updates

Abstract: In order to address power imbalance in large-scale PV systems, this paper presents a multiport isolated medium-frequency (MF) link to process different power levels from PV arrays, using current-fed Z-source inverters (CZSI) modules to drive the energy from the PV array to the MF link in a single power stage. The MF link provides the galvanic isolation required by many codes and standards to integrate a system to the grid. The multiport configuration of the MF link allows the system to process different power levels on each primary port and, being all ports magnetically coupled, provide balanced power levels on secondary ports which can be used for multilevel converters applications. Additionally, the current-fed version of the Z-source topology offers natural protection against short-circuit damage enhancing reliability of the system. The analysis of CZSI cells and the study of asymmetrical power levels transference, as well as simulation and experimental results are presented.

Keywords: photovoltaics; Z-source; current-fed; medium-frequency; power-imbalance

1. Introduction

Since the past two decades, Distributed Energy Sources based on Renewable Energy have grabbed much attention in power transformation and distribution sectors. In particular, solar-photovoltaic (PV) systems have the highest growing rate (along with wind energy) with the addition of 109 GW in 2018–2019 [1]. In terms of installed capacity, PV energy increased from 22 to 489 GW in this decade [2]. The integration of solar energy to the utility grid requires power processing stages in order to successfully inject the gathered energy. The implementation of utility-scale solar systems requires galvanic isolation according to standards in many countries, and it is conventionally implemented by a grid frequency transformer. Even though traditional transformers are reliable and efficient, they are also heavy and bulky [3].

Some approaches for PV systems propose the implementation of Medium-Frequency (MF) isolation in order to reduce volume and weight [3–5]. The topologies with MF links usually features: a DC-AC stage consisting on a DC-DC converter and a DC-AC stage in order to drive the transformer, a Magnetic link operating in medium-high frequency, and an AC-AC stage consisting on a rectifier and a DC-AC stage. The key features of these systems are: individual maximum power point tracking (MPPT), galvanic isolation, enhanced voltage elevation ratio, reduced total harmonic distortion (THD), voltage stress reduction in medium-voltage (MV) stage, and reduced overall system volume and weight. Some drawbacks are: voltage imbalance in multilevel cells due to different power levels in each string, more power stages due to the presence of an additional low voltage inverter and MV rectifier, and increased stress in low voltage stage switches since the all the input power must be handled by a single switch. A solution for multilevel cell imbalance is presented in [3] featuring a MF link that consists on a transformer with several secondary windings which being magnetically coupled *naturally* balances the cascaded cells of the multilevel converter. Some downsides are that the system has four power stages, and reports low global efficiency levels. However, some adjustments in the topology can help improving reliability and efficiency. The PV system low voltage side in [5] consists on a PV string and a DC-AC power stage. The DC-AC power stage requires buck-boost and MPPT capability. DC-AC stage is commonly integrated by a boost converter and an inverter in order to drive the MF transformer [5]. Another approach is stated in [6], proposing a flyback converter plus a H-bridge topology for DC-AC stage features, and enhanced efficiency with high frequency isolation; however, the number of semiconductors and current stress limits the topology to low power applications (<300 W). In [7] a Cuk-SEPIC combination featuring a single switch and coupled inductors is presented in order to obtain a bipolar output enhancing efficiency, however current stressed switch can present reliability problems.

Since PV system behave as current sources, current-fed converters are considered for the DC-AC stage. The isolated current-fed push-pull converter features a low component count and simply circuitry which makes it rather reliable and simple to implement; it also benefits from a high-voltage conversion ratio [8–10]. Some identified drawbacks of the topology are: high switching losses, high-voltage spikes in switches, high start-up current, and central tapped transformer coils requires a bigger core and can be a serious limitation for a magnetically coupled multiport configuration [9,11–13].

The L-type converter is an interesting topology that features reduced current stress in switches and reduced voltage stress on output capacitor and diodes [8,11]. There are a better use of the magnetic core of the MF link and thus making the topology a good option for the multiport implementation. Some limitations of the topology are: higher voltage efforts in switches, voltage spikes in switches due to a resonance with the leakage inductance of the transformer. Current-fed topologies with boost operation also require additional start-up circuitry due to the current in inductors during starting process. The L-type converter is suitable to low voltage, high current applications [8,11].

The Z-source inverter (ZSI) has been considered for DC-AC converters [14,15]; this topology has a buck-boost DC-AC capability in a single-stage which suggests an efficiency and reliability enhancement. The operation principle of the ZSI and current-fed topologies mentioned consist in apply a shoot-through state to overlap the H-bridge branches (0V) which provides natural protection against short-circuits, making it suitable for large-scale applications. After its presentation, variations on the topology were proposed for many applications such a grid-tied converters without galvanic isolation [16–18], with galvanic isolation [19–21], and finally for grid-tied PV systems [22–24].

Z-sources topologies are interesting for PV applications because they can operate as voltage and current source. Additionally, Z-source converters operating as current source can be better applied in medium-high power applications due to the restriction of <1 kV in PV arrays terminals. A current fed Z-source Inverter (CZSI) version is proposed in [25] which features a constant source current, protecting the PV array from returning current.

The CZSI shares many features of the above mentioned topologies such as DC-AC power processing in a single stage and voltage spikes in switches due to resonance with the leakage inductance [12]. Some particular feature of the CZSI in deference to the mentioned topologies is a very low current stress in diode a capacitors, which are the most vulnerable elements on the Z network and thus enhancing the reliability of the circuit. Some drawbacks of the CZSI against the other topologies are the number of passive components and limited voltage boost. Since the PV system voltage does not presents a wide variation, voltage boost drawback is not considered of high relevance. The CZSI has similar to L-type topology power requirements for the magnetic core of the MF link, which is an important feature for multiport applications.

The system considered in this work is shown in Figure 1 and consists in three power stages: Low voltage DC-AC stage consists in a PV array, followed by an elevation stage based on a current-fed Z-source inverter (CZSI) that performs MPPT and sets the voltage for the inverter who will drive the MF link; MF Link is an elevation AC-AC stage which provides multiport configuration integrated by multiple isolated and magnetically coupled inputs and outputs. The MF Link can manage x primary ports and y secondary ports, only restricted by the physical space and power the magnetic core of the transformer can handle. In this study, three input ports where selected since is the minimum number of modules in order to validate that different power levels can be processed in x modules and not only flowing between two modules, and in order to show that output ports are balanced, two ports where selected.

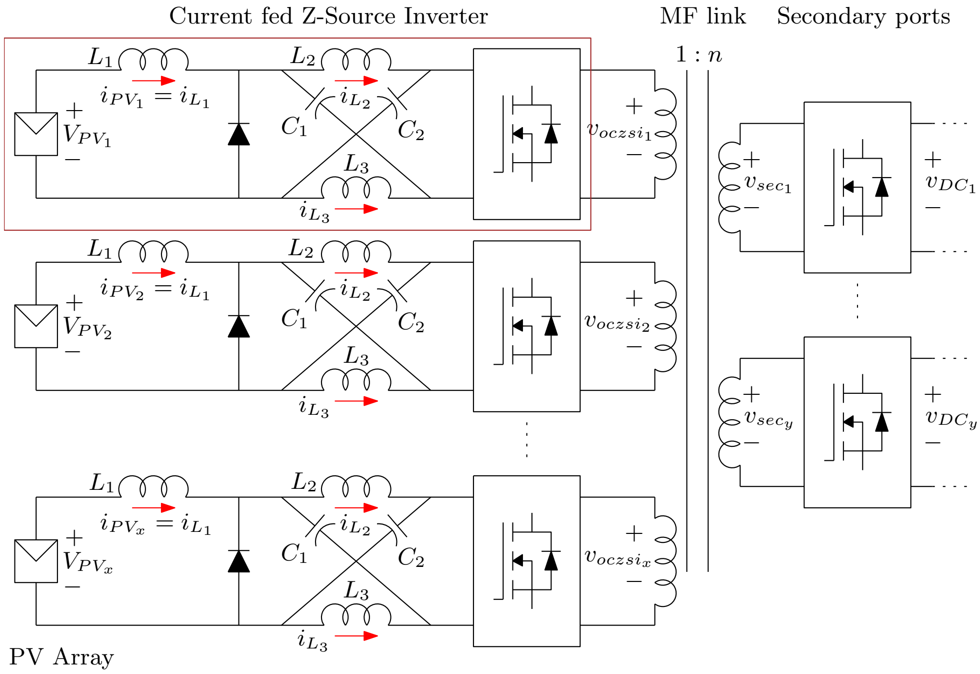

Figure 1. Multiport isolated link system with CZSI input cells to manage asymmetrical power supplies.

The focus of this paper is derived from [26] and presents the analysis of a multiport isolated link in asymmetrical input power transference conditions using CZSI modules to manage the energy. This work shows CZSI analysis, simulation and experimental results to validate the analysis performed. This proposal offers reduction of power stage by using CZSI modules energized by unbalanced PV systems, reliable magnetic isolation with a multiport link to meet standard requirements and, naturally balanced output ports and isolated sources for grid-connected oriented applications.

2. Current-Fed Z-Source Inverter Operation and Design

In Figure 2, the CZSI circuit is presented and Figure 3 shows the equivalent circuits for operation states. In steady state, average voltage in L_1, L_2 and L_3 remains zero as well as current in C_1 and C_2 over a switching period T. The CZSI presents two main operation states: conduction and shoot-through; in conduction state mode (Sw_1 and Sw_4 ON and Sw_2 and Sw_3 OFF, Figure 3a), current across inductors L_1, L_2 and L_3 is given by PV array i_{PV}, and the voltage across the capacitors is set by the PV source V_{PV}. During conduction state, L_3 is charging with V_{PV}, to supply current for the impedance network later.

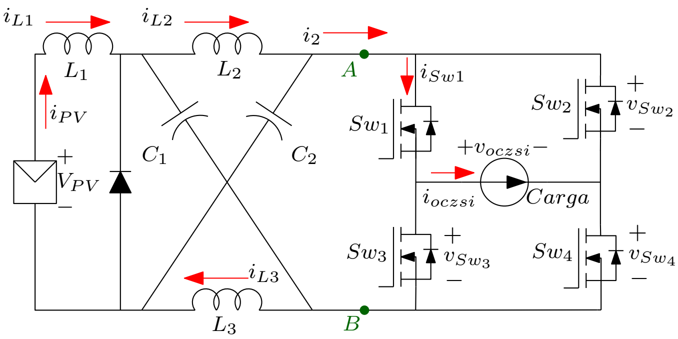

Figure 2. Current-fed Z-source inverter.

In shoot-through state (All switches are ON, Figure 3b), i_{L_1} and i_{L_2} rises as i_{L_3} falls since L_3 supplies the current, i_{PV} remains constant in Δ_{i_L}, limited by inductance L. In this time, voltages in inductors are imposed by v_C. The capacitor voltage decrease in Δ_{v_C} and is limited by a capacitance C. As it can be seen, that the Z LC circuit is always in conduction and the switches are the ones that control operation modes, an hence, the output voltage. The required shoot-through duty cycle D_z for a desired V_{ozp} can be found by the following expression:

$$D_z = 1 - \frac{V_{PV}}{V_{ozp}}, \tag{1}$$

where V_{ozp} is the peak value of v_{oczsi}. The voltage boost for the CZSI is directly modified by D_z; therefore, by manipulating this duty cycle the MPPT can be performed and the DC-AC conversion remains in a single stage.

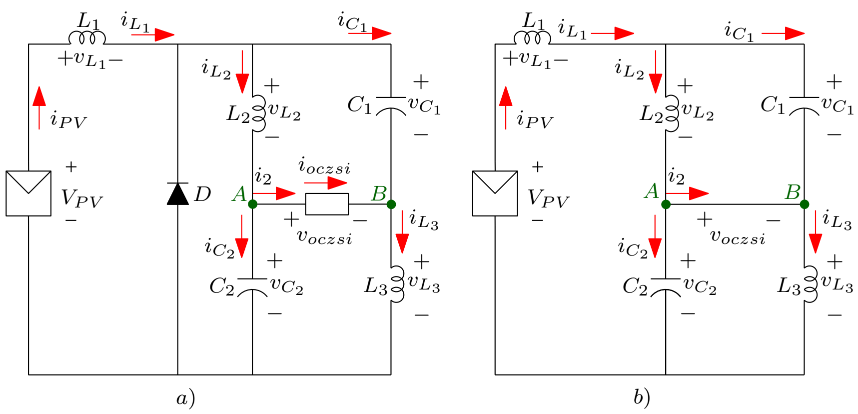

Figure 3. CZSI equivalent circuits: (**a**) CZSI conduction state, (**b**) CZSI shoot-through state.

Output voltage can be obtained through Equation (1), as it is a function of D_z; higher values of D_z produces higher gain limited to $2V_{PV}$. v_{oczsi} RMS voltage is obtained by:

$$V_{oRMS} = V_{ozp}\sqrt{1 - D_z}. \tag{2}$$

The shoot through time TD_z is shared by all of the modules due to the parallel connection, thus if one of the windings is in OV, the rest will be in OV as well. The last results in all of the windings sharing the duty cycle D_z at the higher value.

The effect of D_z in switches is that during $t = [0 \quad T - D_zT]$, half of the current i_2 given by:

$$i_2 = 2i_{L_2} - i_{L_1}, \tag{3}$$

is conducted by all switches. During $t = [T - D_z T \quad T]$, current in switches is i_2. In conduction mode, i_{oczsi} has a ripple Δi_o with a slope given by:

$$m = \frac{\Delta i_o}{\Delta_t} = \frac{I_A - I_B}{\Delta_t}, \tag{4}$$

where I_A and I_B are peak values of i_2 (Figure 4). However, i_{oczsi} is affected by winding impedance Z composed by the leakage inductance L_p and the winding resistance, producing a non-zero current $i_{oczsi} = i_{L_p}$ (Figure 4). The RMS current for i_{oczsi} is given by:

$$I_{oRMS} = \sqrt{\frac{1}{T}\int_0^{T-D_zT} (mT + I_A)^2 dt + \int_{T-D_zT}^{T} i_{Lp}^2 dt}. \tag{5}$$

By solving Equation (5), I_{oRMS} is given by:

$$I_{oRMS} = \sqrt{(i_{PV}^2 + \frac{3}{4}\Delta i_L^2)(1 - D_z) + i_{Lp}^2 D_z}, \tag{6}$$

where I_A is the upper i_2 value, I_B the lower value, and L_p the leakage inductance.

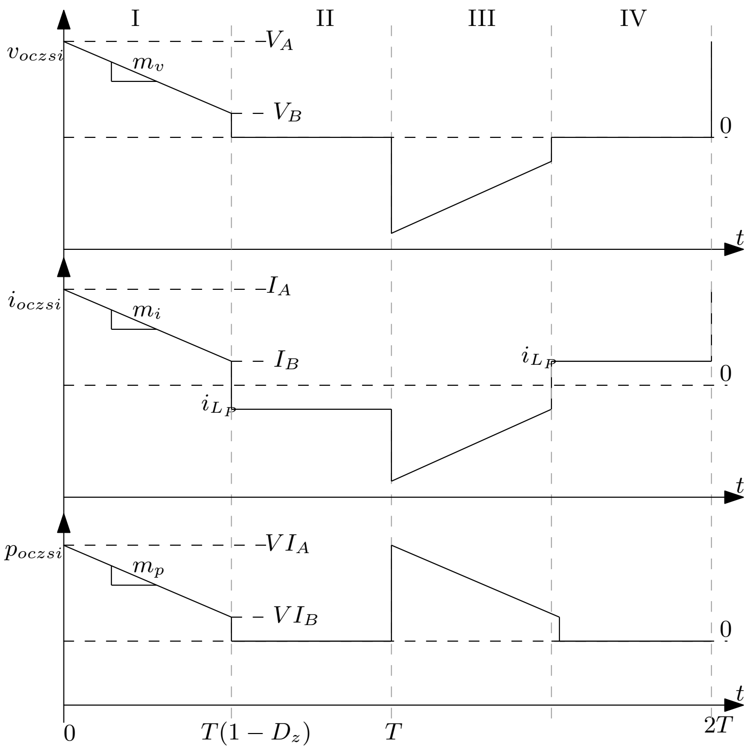

Figure 4. CZSI Output: V_{oczsi}, i_{oczsi}, and power p_{oczsi}.

In Figure 5a, a simplified representation of a multiport configuration consisting on x primary windings transformer and a single output is shown. Voltages V_1, V_2 through V_x are the RMS value of CZSI modules output voltage V_{oczsi}, and V_m is the secondary voltage v_{sec}. In the MF link, the sum of average power supplied to each primary port must match the average power on the secondary ports, thus for a single output:

$$P_1 + P_2 + ... + P_x = P_{sec}, \tag{7}$$

expanding the concept to y secondary ports, the sum of the average power on each secondary output must also match the sum of the average input power:

$$P_1 + P_2 + ... + P_x = P_{sec_1} + P_{sec_2} + ... + P_{sec_y}. \tag{8}$$

For multilevel converters applications, it can be considered that power in each secondary port is balanced since they all have the same number of turns and the same output voltage. Secondary ports also share the same current since the all supply the same load, thereby Equation (8) can be expressed as:

$$P_1 + P_2 + ... + P_x = yP_{sec}. \tag{9}$$

The parallel configuration shows that when a module is in shoot-through state, the remaining modules will share this state, thus voltage v_{oczsi} will be zero for all of the windings, resulting in an identical equivalent D_z value for all input CZSI modules. The last implies that all the cells will have very similar values of v_{oczsi}.

The imposed duty cycle D_z will be the higher value of all CZSI modules for the MPP, thus having different D_z references is not necessary. Current levels will be in function of the power supplied by the PV array, thus different in all primary ports.

Despite the different power levels on the modules, the non-zero current associated to L_p, remains similar for all windings since it is product of parasitic elements, and it is assumed that all windings are homogeneous.

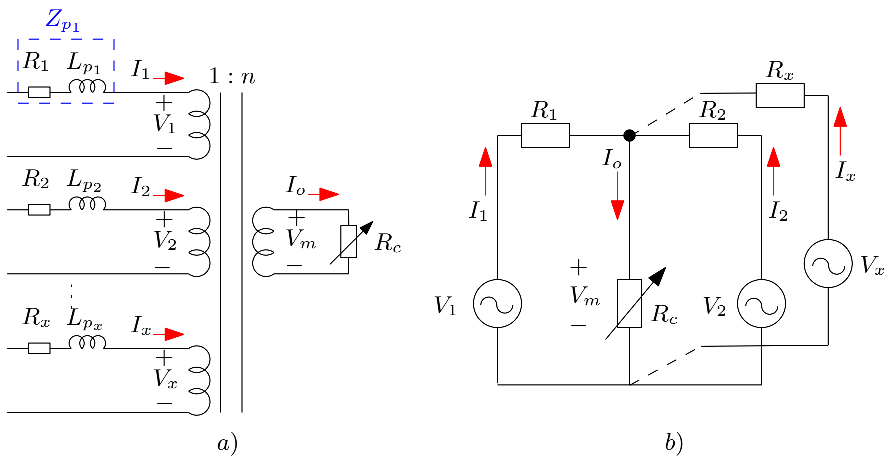

Figure 5. (**a**) Multiport transformer, (**b**) Equivalent circuit.

Semiconductor Sizing for CZSI Modules

The voltage and current stress on semiconductors are defined by the operation mode of the CZSI module. The voltage stress for the semiconductors on CZSI conduction mode, is the voltage v_{ozp} and can be found with Equation (1) and zero for shoot-through mode:

$$v_{Sw} = \begin{cases} v_{ozp} & 0 \leq t < T(1-D_z) \\ 0 & T(1-D_z) \leq t \leq T. \end{cases} \tag{10}$$

For selection purposes, a security factor of 50% can be added to v_{ozp} and is given by:

$$V_{Sw_{selec}} = V_{ozp}1.5 = \left(V_{PV} \frac{1}{1-D_z} \right) 1.5. \tag{11}$$

The current across the semiconductors, also depends on operation mode and can be expressed by:

$$i_{Sw} = \begin{cases} i_2 & 0 \le t < T(1 - D_z) \\ i_2/2 & T(1 - D_z) \le t \le T. \end{cases} \tag{12}$$

The maximum current that semiconductors must conduct is the peak value of i_2 plus a security factor of 25%. The current to be considered when choosing a device is given by:

$$I_{Sw_{selec}} = i_{2_{max}} = \left(I_{PV} + \frac{3\Delta i_L}{2} \right) 1.25. \tag{13}$$

3. Power Transfer under Unbalanced Conditions

An issue of having the whole installed capacity divided in strings is that the power in each array of PV panels can be unbalanced. Let's consider a two input modules scenario, where P_1 and P_2 are CZSI modules output power and are different from each other.

A simple scheme is given in Figure 5b for analysis purposes. Resistance R is considered equal for all windings and thus $R_1 = R_2 = R$. From Figure 5b, the voltage on the secondary side can be computed by:

$$V_1 n - I_1 R = V_m = V_2 n - I_2 R, \tag{14}$$

where n is the turn ratio and, V_1 and V_2 are the RMS values of v_{oczsi} in modules 1 and 2 respectively. Such voltages cannot be arbitrary set to extract two different power levels on each loop, since (14) has to be fulfilled. If the voltage V_1 is imposed, then V_2 will be in function of the desired power, thus V_2 is a variable voltage source. To find a combination of V_1 and V_2, that will allow different power transfer on modules, first V_m must be found in terms of V_1 with (14). Then P_2 can be computed from:

$$P_2 = \frac{R}{n} I_2^2 + \frac{V_m}{n} I_2. \tag{15}$$

By solving (15) for I_2, a voltage value for V_2 to transfer P_2 can be found. For more than two modules or windings, a similar analysis can be performed. One module has a fixed voltage, and all the subsequent modules adapt their voltage to meet the power transference needed.

$$V_1 n - I_1 R = V_m = V_2 n I_2 R = ... = V_x n I_x R. \tag{16}$$

Therefore the current for x given modules, (17) can be solved for I_x:

$$P_x = \frac{R}{n} I_x^2 + \frac{V_m}{n} I_x. \tag{17}$$

Once expressions for output voltage and current are given, power on each winding can be calculated. Based on Figure 4, the average power is given by:

$$P = \frac{1}{T} \int_0^{T - TD_z} VoI_B + \frac{V_o(I_A - I_B)}{2} t(dt), \tag{18}$$

$$P = \frac{V_o(I_A + I_B)}{2} (1 - D), \tag{19}$$

where I_A and I_B are the upper and lower I_2 values respectively. Apparent power S is expressed by:

$$S = V_{oRMS} \sqrt{(i_{PV}^2 + \frac{3}{4} \Delta i_L^2)(1 - D_z) + i_{Lp}^2 D_z}. \tag{20}$$

From (20) it can be observed that the $i^2_{Lp}D_z$ component is associated to reactive power, and since all cells have similar values of L_p (because all windings are identical) the component in $i^2_{Lp}D_z$ will be the same for all modules, an thus, have similar reactive power levels on all cells despite power level.

4. Results

Once the operation principle has been presented and the design equations given, simulation studies in PSIM, and experimental tests were performed with the parameters shown in Table 1. Simulations were performed considering the schematic in Figure 1; a PV system with a MF link including 3 primary ports and 2 secondary ports with a turn ratio of 1:7. A variable DC load is applied to each secondary port in order to extract 300 W from each PV array to get a total output power of 900 W, also, each CZSI module has a switching frequency ok 20 kHz with an input voltage of 50 V.

After the validation through simulations, a prototype has been built. The experimental prototype consists in two input CZSI modules energized by a PV array of two 250W PV panel in order to get a total power of 500 W and 50 V input voltage at MPP. Turn ration in the multiport transformer and D_z reference parameters were retained from simulation studies.

4.1. Simulation Results

In first instance, the system's performance was evaluated under balanced conditions using a PV array of 2 panels in series obtaining 50 V, 6.6 A, 300 W with an irradiance of 1 kW/m^2 applied to each CZSI module, and a variable load is applied to each secondary port in order to extract the maximum power around 900 W. In Figure 6 the voltage v_{oczsi} on modules 1, 2 and 3 are presented, and it can be see that they have a v_{ozp} value of 80 V. In the secondary side, the voltages v_{sec_1} and v_{sec_2} shows the same waveform with the voltage gain due to MF link's turn ratio, an thus the voltage in all of the ports remains balanced. From Equation (1), the voltage in conduction mode can be estimated in 80 V for the V_{PV} in the simulation, and from Equation (2), its RMS value of 62.3 V can be found.

Table 1. Simulation and experimental parameters.

Parameters	Simulation	Experimental
Module output power	300 W	300 W
Total power	900 W	600 W
Irradiance	1000 W/m^2	unknow
Input voltage (V_{PV})	50 V	50 V
CZSI module output voltage (V_{ozp})	80 V	80 V
Secondary ports voltage (v_{sec})	560 V	560V
Duty cycle (D_z)	0.37	0.37
L_1, L_2 and L_3	0.38 mH	0.38 mH
C_1 and C_2	2 μF	2 μF
Switching frequency	20 kHz	20 kHz
Primary ports	3	2
Secondary ports	2	2
MF link turn ratio	1:7	1:7
Primary leakage inductance (L_p)	1.18 μH	1.18 μH
Secondary leakage inductance (L_s)	37.7 μH	37.7 μH
Primary parasitic resistance (R_p)	45 mΩ	45 mΩ
Secondary parasitic resistance (R_s)	1.59 Ω	1.59 Ω
Magnetizing inductance (L_m)	2 mH	2 mH

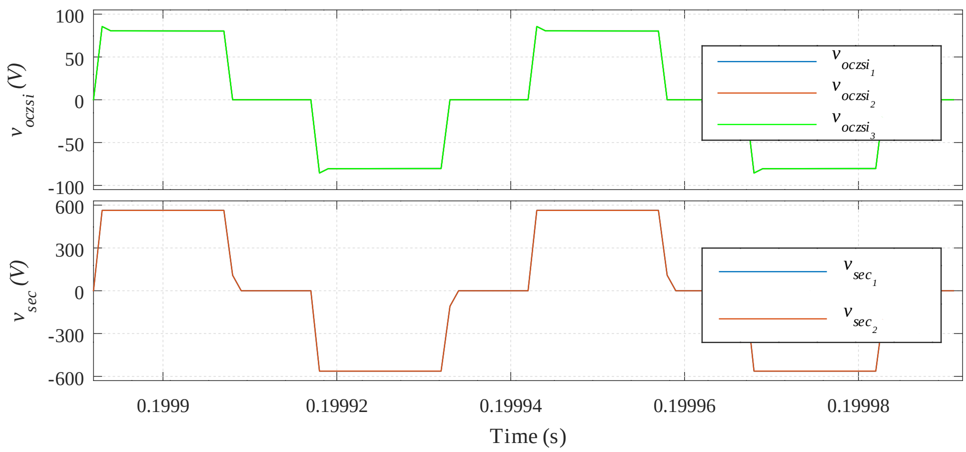

Figure 6. Simulation results: CZSI modules output voltages v_{oczsi_1}, v_{oczsi_2}, v_{oczsi_3} and secondary ports voltages v_{sec_1} and v_{sec_2} under balanced conditions.

Since the study is in balanced power conditions, the same current i_{oczsi} is expected on the three CZSI modules and RMS value can be estimated from Equations (3) and (6) to be around 5.6 A and 4.8 A respectively. Figure 7 validates that under balanced conditions the current on primary modules are equal. It can be observed that during shoot-through times, there is a non-zero current on CZSI modules output and in conduction mode. On the other hand, the current on the secondary ports, does not present non-zero current in shoot-through times and thus the effect of parasitic elements on MF link are decoupled from primary side.

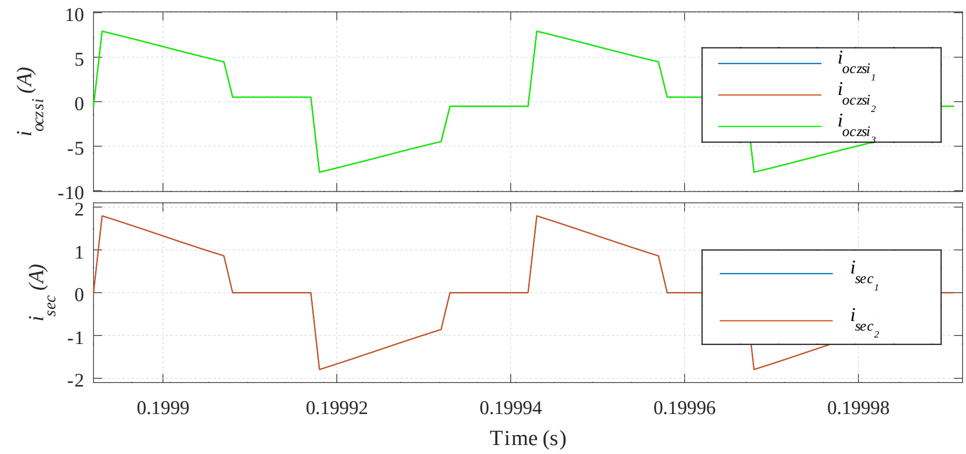

Figure 7. Simulation results: CZSI modules output current i_{oczsi_1}, i_{oczsi_2}, i_{oczsi_3} and secondary ports currents i_{sec_1} and i_{sec_2} under balanced conditions.

Figure 8 presents the average power on primary and secondary ports. First, the average output power on CZSI modules are shown in the first graphic and all of them are overlapped as expected for balanced conditions. In the same fashion, the average power in secondary side is balanced in both secondary outputs, and finally it can be observed that the sum of the average power of the three CZSI modules, matches with the sum of the average power on the secondary ports, and the difference between both is attributed to parasitic resistance in the MF link.

Once the operation under balanced conditions are validated, power imbalance studies were carried out. In order to appreciate the power imbalance, different irradiance were applied to each CZSI module: 900 W/m^2 for module 1, 500 W/m^2 in module 2, and 300 W/m^2 to module 3. Variable loads were kept on each secondary output in order to obtain the maximum power extraction. Also a fixed 0.37 D_z in all modules was set to put the system in MPP; since the higher D_z is imposed to all coupled modules, a master-slave configuration is used, selecting the module with higher irradiance as the master.

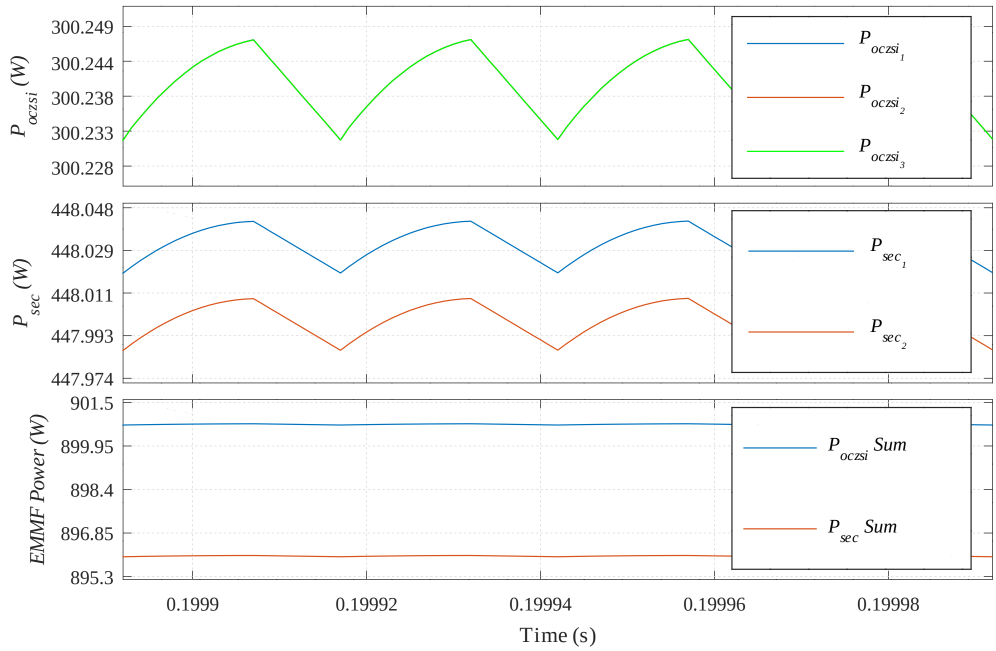

Figure 8. CZSI simulation results: Average power in primary ports and average power in secondary ports under balanced power operation.

Voltages in primary and secondary ports in steady state are shown in Figure 9. Voltage in primary ports are the output of CZSI modules and all three of them presents the same v_{oczsi} value of 80 V during conduction state, and zero voltage in shoot-through states despite the imbalance applied. Similarly, the voltage on the secondary side has the same waveform with the gain of the MF link in the magnitude, passing from 80 V peak on primary side to 560 V peak on the secondary side. This validates that voltage balance is kept in primary and secondary ports despite power imbalance.

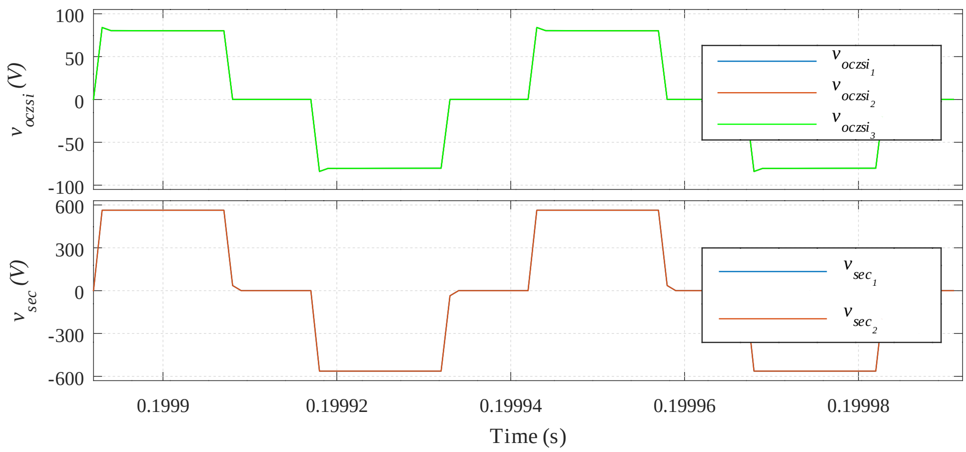

Figure 9. Simulation results: CZSI modules output voltages v_{oczsi_1}, v_{oczsi_2}, v_{oczsi_3} and secondary ports voltages v_{sec_1} and v_{sec_2} under unbalanced conditions.

Figure 10 shows the steady state current on primary and secondary ports and it can be observed that currents i_{oczsi_1}, i_{oczsi_2} and i_{oczsi_3} are different in function of the power supplied by the corresponding PV array. The non-zero current can be see during shoot-through state produced by parasitic elements in MF link. Considering, all primary ports have the same voltage, and each one has different current values, it validates that each port is managing different power levels. Despite the imbalance in CZSI modules, the second graphic shows that the current on secondary ports are equal without non-zero current during shoot-through states, which validates a balanced and decoupled power on secondary ports.

Figure 11 shows the power in primary ports as well as the average power in secondary ports. It can be see that each module has a different average power in primary side, in contrast to the secondary side that has exactly the same average power in both secondary ports.

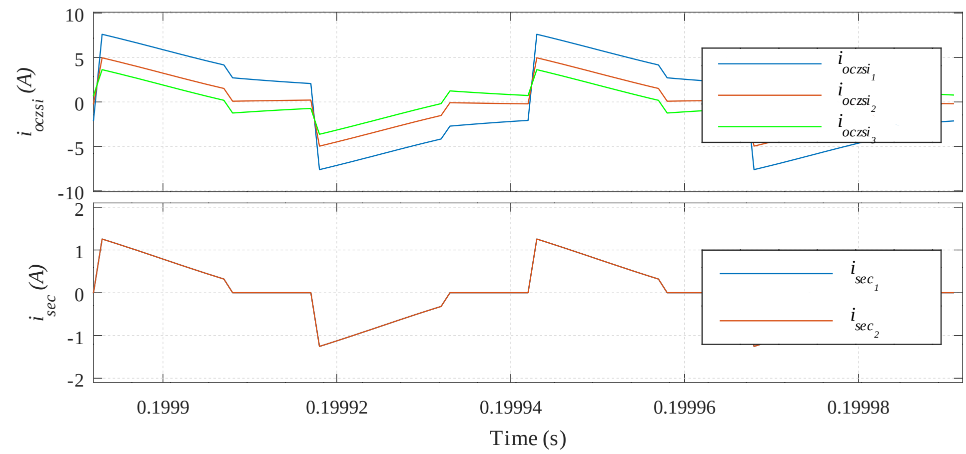

Figure 10. Simulation results: CZSI modules output current i_{oczsi_1}, i_{oczsi_2}, i_{oczsi_3} and secondary ports currents i_{sec_1} and i_{sec_2} under unbalanced conditions.

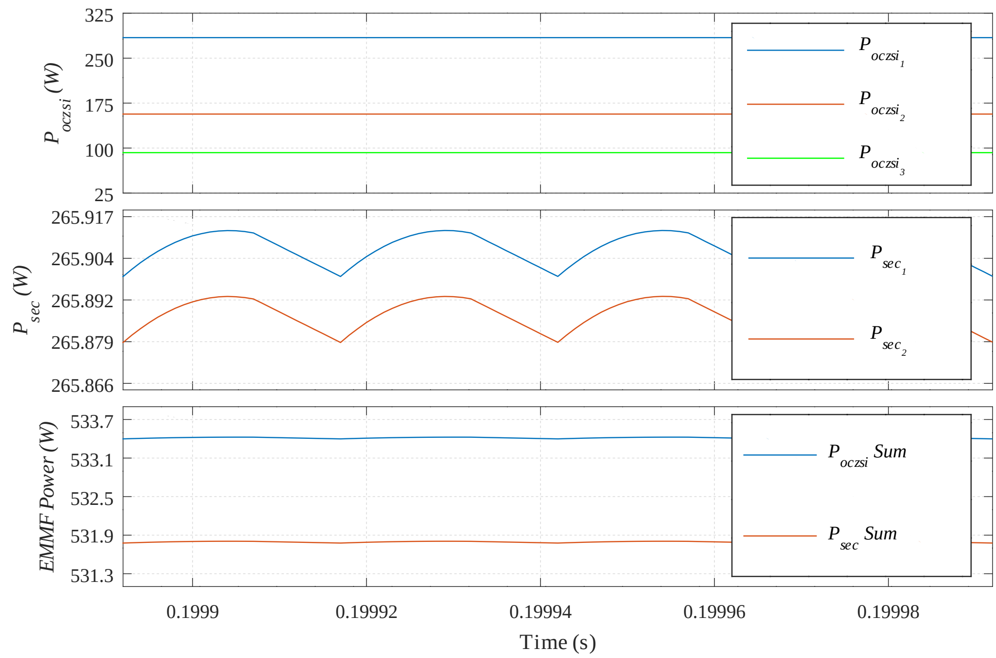

Figure 11. CZSI simulation results: Average power in primary ports and average power in secondary ports under unbalanced power operation.

When comparing the sum of the average power on primary and secondary side it is basically the same, but similar to balanced conditions, a small difference can be observed due to leakage inductance which produces the non-zero current present in primary side but not in secondary side. Finally a summary of the results obtained in the simulation studies is presented in Table 2.

Table 2. Simulation results.

Parameters	Primary Port 1	Primary Port 2	Primary Port 3	Secondary Port 1	Secondary Port 2
Balanced					
RMS Voltage	62.3 V	62.3 V	62.3 V	436 V	436 V
RMS Current	4.8 A	4.8 A	4.8 A	1.03 A	1.03 A
Output Power	300 W	300 W	300 W	448 W	448.3 W
Unbalanced					
RMS Voltage	62.3 V	62.3 V	62.3 V	436 V	436 V
RMS Current	4.56 A	2.51 A	1.48 A	0.646 A	0.646 A
Output Power	284.4 W	156.7 W	92.3 W	265.9 W	265.8 W

4.2. Experimental Results

Once the CZSI modules and MF link were validated through simulations, an experimental prototype has been tested in multiport configuration. The prototype is shown in Figure 12 and consists in 2 input CZSI modules, a magnetic link and two secondary cells with a diode full-wave rectifier on the output. The MF link consist on a multiport transformer with 15 turns on each primary port and 106 turns on each secondary port, built in a N27 E-80 ferrite core. Each CZSI module is energized by a PV panel array consisting on two 30 V, 8,33 A, 250 W panels connected in series achieving 60V at its MPP. Tests were carried out applying a 940 Ω resistive load to the output in order to demand 470 W at MPP. The CZSI modules were operated with a fixed D_z as marked in Table 1, but due to ambient conditions, only 60% of the array power was produced. Despite the last, tests validates the behavior of the system with a PV system supply.

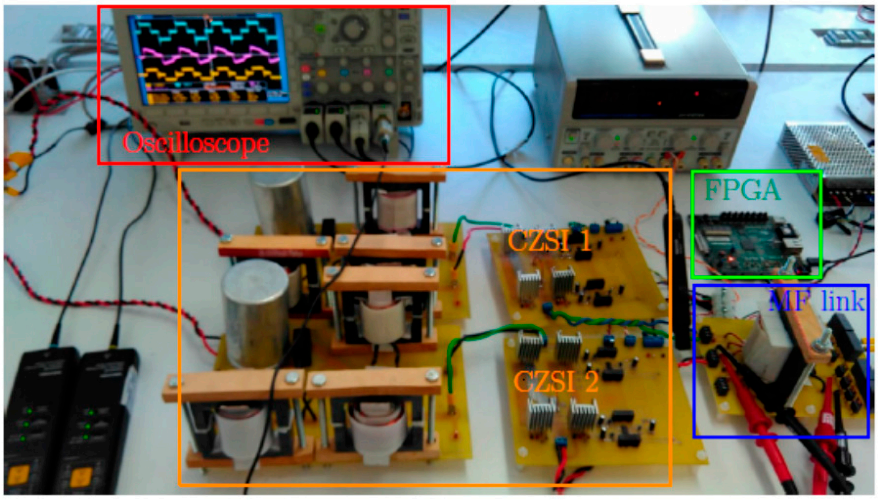

Figure 12. Experimental prototype.

In Figure 13 the performance of the prototype under balanced conditions is shown. The currents i_{oczsi_1} and i_{oczsi_2} are on channels 1 and 3 respectively, it can be see that they are overlapped with very small variations with a peak value of 7.5 A and 7.3 A on conduction mode, giving an approximate RMS value of 5 A; it can be noticed that the values are consistent with the simulation presented in Figure 7 with a peak value around 7.5 A and descending to 4.5 A. A high-frequency component oscillation due to a resonance between the leakage inductance of the MF link and the parasitic capacitance of the MOSFET can be appreciated during shoot-through times. In channels 2 and 4, voltages v_{oczsi_2} and v_{oczsi_2} are shown and are also equal with a v_{ozp} near to 75 V for a more-less 60 V RMS on both modules. The v_{oczsi} values obtained are similar to the ones presented in Figure 6 and the behavior is consistent showing a small spike during conduction state. The similar values of both CZSI values confirm that both PV systems are in a balanced state. In balanced state, both modules extracted 300 W from each PV array for a 600 W output power.

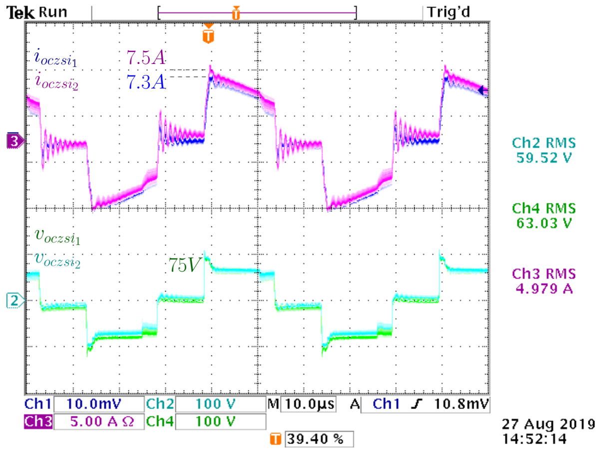

Figure 13. System test under balanced conditions. Ch1 (10 mV/div=5 A/div): i_{oczsi_1}, Ch3 (5 A/div): i_{oczsi_2}, Ch2 (100 V/div): v_{oczsi_1} and Ch4 (100 V/div): v_{oczsi_2}.

Once the performance of the prototype was validated in balanced conditions, a test under power imbalance was performed using the same two PV panels arrays of the balanced test. The resistive load and D_z duty cycle was also kept the same as before. Additionally, partial shade was applied to the PV panel array in module 2 in order to introduce the power imbalance.

In Figure 14, current i_{oczsi} in module 1 and 2 can be observed on channel 1 and 3 respectively. It can be noted that the same high frequency oscillation due to resonance between MOSFET's parasitic capacitance and the leakage inductance of the MF link in Figure 13 is also present under unbalanced conditions. Different current levels can be clearly appreciated, with 7.2 A peak on i_{oczsi_1} and 6 A peak on i_{oczsi_2}. Despite both cells have different current levels, v_{oczsi} stays on the same level as in balanced condition with 75 V v_{ozp}. A non-zero current in i_{oczsi} during shoot-through times can be observed and is related to the parasitic elements of the transformer.

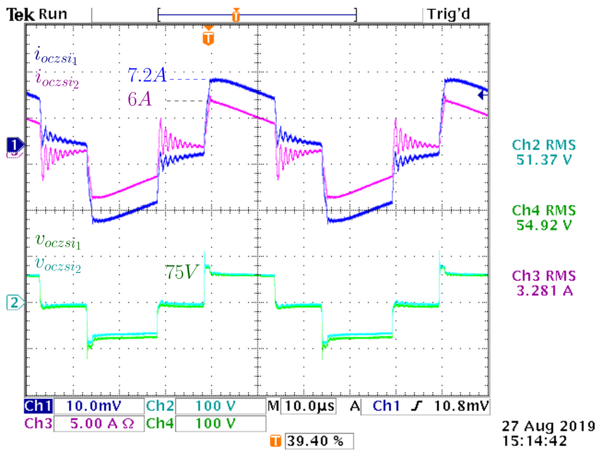

Figure 14. Multiport power imbalance test. Ch1 (10 mV/div=5 A/div): i_{oczsi_1}, Ch3 (5 A/div): i_{oczsi_2}, Ch2 (100 V/div): v_{oczsi_1} and Ch4 (100 V/div): v_{oczsi_2}.

In Figure 15 power in primary and secondary ports are presented. The first and second waveforms were taken after the diode full-wave rectifier and correspond to power in secondary ports 1 and 2 respectively; it can be see that they are equal in magnitude. The third and fourth waveform are the power in CZSI module 1 and 2 respectively, observe that they have different power levels and the sum matches the sum of power in the secondary side. The last validates that a balanced output can be generated despite power imbalances in the MF link inputs.

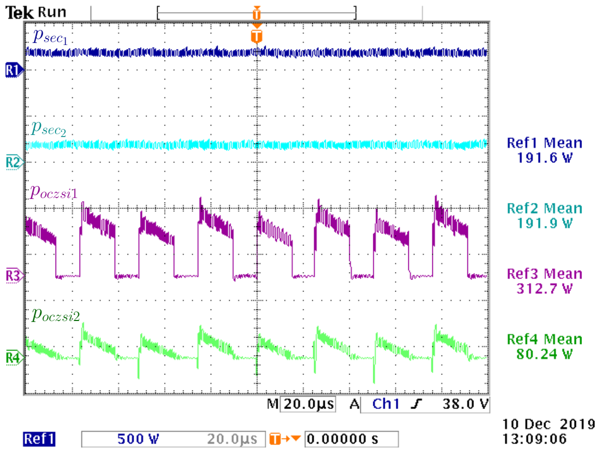

Figure 15. Multiport power imbalance test. Ch1 (500 W/div): output power in secondary port 1 p_{sec_1}, Ch2 (500 W/div): output power in secondary port 2 p_{sec_2}, Ch3 (500 W/div): output power in CZSI module 1 p_{oczsi_1}, and output power in CZSI module 2 Ch4 (500 W/div): p_{oczsi_1}.

5. Discussion

From both simulation an experimental results, it was shown that current and voltage stress was kept in reasonable levels and only switches were affected by a voltage transitory. The last, is also present in boost-HB topologies, however over-current peaks are not present in CZSI as can be seen in Figures 13 and 14, which suggest a lower current stress in semiconductor devices. In addition the shoot through operation gives more time to react to faults related to gate signals in switches: if the gate signals are lost due to external factor like irradiated noise from MF link or processor damage, the switches will be protected by the Z-source by limiting current until a protection flag is enabled. On the other hand, boost-HB topologies will just be damaged in case of losing gate signal, and thus suggesting that the CZSI enhance the reliability of the system.

For unbalanced power conditions, it can be seen that voltage between all PV arrays terminals remains similar for all the ports. However current supplied to each CZSI modules is different and is a function of the power supplied by the corresponding PV array. The voltage remains similar for all CZSI modules, as shown in simulation and experimental results. The current is the parameter that changes for the primary modules and thus the one that validates the transfer of different power levels in primary ports as shown in Figures 10 and 13.

Despite the unbalanced power levels of the primary modules, the voltage is the same in secondary ports, but also the current is the same and thus the power on secondary side is balanced without additional actions, or modulation taken. The last is particularly useful for multilevel inverter applications where multiple isolated and balanced sources are required for proper operation. Topologies with galvanic isolation previously reported, usually implement multiple single-input single-output transformers in order to manipulate strings individually, this allows to follow MPP on each PV array and drive the transformer. However this produce different output on secondary side for each string and thus requires to be balanced by some added control strategy.

6. Conclusions

A multiport scheme with CZSI modules to manage unbalanced power conditions was introduced in this paper. The operation principle of the CZSI was presented as well as the design equations to size CZSI components. An analysis of the multiport operation under unbalanced conditions was given. In this scheme, the CZSI was able to drive power from a PV array to the MF link in a single stage. Buck-boost operation of the CZSI modules is achieved by controlling the shoot-through time. CZSI has the limitation that it only has the duty cycle as a freedom degree and thus MPPT can only be achieved by manipulating this parameter. However, by operating as a current-fed converter, the CZSI modules can operate at similar voltage levels and managing a wider difference between the current levels which make this converter a feasible alternative for PV applications. Simulation and experimental studies were performed in balanced and unbalanced conditions, confirming that this multiport scheme can manage different power levels form PV arrays on its primary side, at the time it generates isolated and balanced outputs on the secondary ports, making it suitable for multilevel converter applications.

Author Contributions: Formal analysis, J.M.S. and V.C.; Investigation, J.M.S. and M.G.G.; Methodology, J.M.S., M.A.B. and J.A.; Project administration, V.C.; Supervision, V.C.; Writing – original draft, J.M.S.; Writing – review & editing, V.C. and J.A. All authors have read and agreed to the published version of the manuscript.

Funding: This research work was supported by the project UASLP-TRAFOS SLP 252557. The authors would like to thank The National Council of Science and Technology of Mexico (CONACyT) for the academic scholarship under the grant number 415079.

Acknowledgments: The authors acknowledge to the UASLP Electrical Power Quality and Motor Control Laboratory (LABCEECM) staff for technical and material support during experimental stage.

Conflicts of Interest: The authors declare no conflicts of interest.

References

1. International Renewable Energy Agency. Roadmap to 2050 (2019 edition). In *Global Energy Transformation*; IRENA; 2019; p. 16. Available online: https://www.irena.org/-/media/Files/IRENA/Agency/Publication/2019/Apr/IRENA_Global_Energy_Transformation_2019.pdf (accessed on 30 January 2020)
2. Int. Renew. Energy Agency. Solar-Photovoltaic Statistics. In *Renewable Capacity Statistics 2019*; IRENA; 2019; p. 21. Available online: https://www.irena.org/-/media/Files/IRENA/Agency/Publication/2019/Mar/IRENA_RE_Capacity_Statistics_2019.pdf (accessed on 30 January 2020)
3. Islam, R.M.; Youguang G.; Jianguo Z. A Multilevel Medium-Voltage Inverter for Step-Up-Transformer-Less Grid Connection of Photovoltaic Power Plants. *Trans. Ind. Electron.* **2014**, *4*, 881–889. [CrossRef]
4. Elsayad N.; Osama M. A cascaded high frequency AC link system for large-scale PV-assisted EV fast charging stations. In Proceedings of the 2017 IEEE Transportation Electrification Conference and Expo (ITEC), Chicago, IL, USA, 22–24 June 2017; pp. 90–94. Available online: https://ieeexplore.ieee.org/document/7993252 (accessed on 30 January 2020)
5. Islam, R.M.; Mahfuz-Ur-Rahman A.M. Modular Medium-Voltage Grid-Connected Converter With Improved Switching Techniques for Solar Photovoltaic Systems. *Trans. Ind. Electronics.* **2017**, *64*, 8887–8896. [CrossRef]
6. Zaim, R.; Jamaludin J.; Rahim N.A. Photovoltaic Flyback Microinverter With Tertiary Winding Current Sensing. *Trans. Power Electron.* **2019**, *34*, 7588–7602. [CrossRef]
7. Nathan, K.; Ghosh, S. A New DC-DC Converter for Photovoltaic Systems: Coupled-Inductors Combined Cuk-SEPIC Converter. *Trans. Energy Conversion.* **2019**, *34*, 191–201. [CrossRef]
8. Kim, H.; Yoon, C.; Choi, S. An Improved Current-Fed ZVS Isolated Boost Converter for Fuel Cell Applications. *IEEE Trans. Power Electron.* **2010**, *25*, 2357–2364. [CrossRef]
9. Wu,Q.; Wang, Q.; Xu, J.; Xu, Z. Active-clamped ZVS current-fed push–pull isolated dc/dc converter for renewable energy conversion applications. *IET Power Electron.* **2018**, *11*, 373–381. [CrossRef]
10. Ohtsu, S.; Yamashita, T.; Yamamoto, K. Stability in high-output-voltage push–pull current-fed converters. *IEEE Trans. Power Electron.* **1993**, *8*, 135–139. [CrossRef]
11. Wolfs, P.J. A current-sourced DC-DC converter derived via the duality principle from the half-bridge converter. *IEEE Trans. Ind. Electron.* **1993**, *40*, 139–144. [CrossRef]
12. Nguyen, M.-K.; Duong, T.-D; Lim, Y.-C.; and Choi, J.-H. Active CDS-clamped L-type current-Fed isolated DC-DC converter. *J. Power Electron.* **2018**, *4*, 955–964.
13. De Aragao Filho, W.C.P.; Barbi, I. A comparison between two current-fed push-pull DC-DC converters-analysis, design and experimentation. In Proceedings of the International Telecommunications Energy Conference 1996, Boston, MA, USA, 6–10 October 1996; pp. 313–320. Available online: https://ieeexplore.ieee.org/document/573330 (accessed on 30 January 2020)
14. Guisso, R.A.; Andrade, A.M.S.S. Grid-tied single source quasi-Z-source cascaded multilevel inverter for PV applications. *Electron. Lett.* **2019**, *55*, 42–343. [CrossRef]

15. Andrade, A.M.S.S.; Guisso, R.A. Quasi-Z-source network DC–DC converter with different techniques to achieve a high voltage gain. *Electron. Lett.* **2018**, *54*, 710–712. [CrossRef]
16. Liu, Y.; Ge, B.; Abu-Rub, H.; Sun, H. Hybrid Pulsewidth Modulated Single-Phase Quasi-Z-Source Grid-Tie Photovoltaic Power System. *Trans. Ind. Informatics* **2016**, *12*, 621–632. [CrossRef]
17. Choi, W.-Y.; Yang, M.-K. Transformerless Quasi-Z-Source Inverter to Reduce Leakage Current for Single-Phase Grid-Tied Applications. *Electronics* **2019**, *8*, 312. [CrossRef]
18. Wang, B.; Tang, W. A Novel Three-Switch Z-Source SEPIC Inverter. *Electronics* **2019 8**, 247. [CrossRef]
19. Rahul, J.R.; Kirubakaran, A. Single-Phase Quasi-Z-source based Isolated DC/AC converter. In Proceedings of the IEEE International Conference on Power Systems (ICPS), New Delhi, India, 4–6 March 2016.
20. Liu, Y.; Abu-Rub, H.; Ge, B. Front-End Isolated Quasi-Z-Source DC–DC Converter Modules in Series for High-Power Photovoltaic Systems—Part I: Configuration, Operation, and Evaluation. *Trans. Ind. Electron.* **2017**, *64*, 347–358. [CrossRef]
21. Ahmed, H.F.; Cha, H. A New Class of Single-Phase High-Frequency Isolated Z-Source AC–AC Converters With Reduced Passive Components. *Trans. Power Electron.* **2018**, *33*, 1410–1419. [CrossRef]
22. Sajadian, S.; Ahmadi, R. ZSI for PV systems with LVRT capability. *IET Renew. Power Gen.* **2019**, *12*, 1286–1294. [CrossRef]
23. Uno, M.; Shinohara, T. Module-Integrated Converter Based on Cascaded Quasi-Z-Source Inverter With Differential Power Processing Capability for Photovoltaic Panels Under Partial Shading. *Trans. Power Electron.* **2019**, *34*, 11553–11565. [CrossRef]
24. Liu, J.; Wu, J.; Qiu, J.; Zeng, J. Switched Z-Source/Quasi-Z-Source DC-DC Converters With Reduced Passive Components for Photovoltaic Systems. *IEEE Access* **2019**, *7*, 40893–40903. [CrossRef]
25. Anderson, J.; Peng, F.Z. Four quasi-Z-Source inverters. In Proceedings of the 2008 IEEE Power Electronics Specialists Conference, Rhodes, Greece, 15–19 June 2008.
26. Sandoval, J.M.; Cardenas, V. Current-Fed Z-Source Converter for Medium-Voltage Medium-Frequency Isolated Solar-Photovoltaic Systems. In Proceedings of the 2019 IEEE Applied Power Electronics Conference and Expo, Anaheim, CA, USA, 17–21 March 2019.